Thermomechanical anomalies and polyamorphism in B_2O_3 glass: A molecular dynamics simulation study

Liping Huang and John Kieffer*
Department of Materials Science and Engineering, University of Michigan, Ann Arbor, Michigan 48109-2136, USA
(Received 29 June 2006; published 20 December 2006)

Molecular dynamics (MD) simulations, based on a new coordination-dependent charge-transfer potential, were used to study the behavior of B_2O_3 in response to various thermal and mechanical constraints. This interaction potential allows for the charges on atoms to redistribute upon the formation and rupture of chemical bonds, and dynamically adjusts to multiple coordination states for a given species. Our simulations reveal the structural origin of the anomalous thermomechanical behaviors of B_2O_3, such as the increase of mechanical moduli upon expansion of the structure. While this phenomenon has been experimentally observed in the glass just below T_g and in the molten state above 800 °C, our simulations predict for the first time that the mechanical moduli of B_2O_3 glass also increase upon expansion under tensile stress. These anomalous behaviors can be explained as the result of localized structural transformations between two motifs of different stiffness that are similar to those found in the material's crystalline counterparts. The mechanism we found for B_2O_3 is analogous to the one we identified earlier as underlying the anomalous behaviors of SiO_2, and appears to be universal for network-forming glasses. Furthermore, our simulations led us to the discovery of new low-density B_2O_3 crystals, which provide a key to understanding the anomalous thermomechanical behaviors of vitreous B_2O_3 and the crystallization anomaly of this compound.

DOI: 10.1103/PhysRevB.74.224107 PACS number(s): 64.70.−p, 65.60.+a, 61.43.Fs, 62.20.−x

I. INTRODUCTION

The glass-forming ability in oxides is commonly associated with the formation of a three-dimensional random network. Structural units in compounds such as SiO_2, GeO_2, and B_2O_3, afford the flexibility to arrange in ways that satisfy bonding requirements and span space continuously without the need for the regular packing that is characteristic of crystals. Perhaps as one manifestation of their unique topologies, these network structures exhibit a number of anomalous behaviors. For example, amorphous silica exhibits negative thermal expansion (NTE) in two different temperature regimes, near absolute zero[1] and in the molten state.[2] Furthermore, the elastic modulus of silica glass decreases with increasing pressure, reaching a minimum at around 3 GPa. Conversely, the modulus increases with increasing temperature or under tensile stress.[3] In other words, the elastic modulus increases when the structure expands and decreases when the structure contracts. Based on our previous simulations we were able to explain this phenomenon as the result of localized structural transitions between two different configurations of network rings without breaking any bonds, essentially echoing the transformation between the α- and β-modification of cristobalite, one of the crystalline forms of silica.[3–6] Accordingly, the anomalous thermomechanical behaviors in vitreous silica are the manifestation of one of two types of polyamorphic transitions (i.e., the changeover between two thermodynamically and structurally distinct noncrystalline state of a given substance).[7–18] While the one responsible for these anomalies is reversible, the other type, which is predominantly invoked by applying pressure, involves bond breaking and reformation and leads to irreversible densification of the glass structure.

From Brillouin light scattering experiments we have learned that the anomalous increase of the elastic modulus with temperature is ubiquitous to all three of the aforementioned network glass formers.[19] In SiO_2 the modulus increases continuously, and the transition between glass and liquid is at best apparent through a minute change in the slope of the modulus vs temperature data. In GeO_2, T_g can be identified by a small but distinct cusp in the modulus vs temperature data, i.e., the modulus decreases slightly above T_g, but quickly regains a positive temperature dependence. In contrast, for B_2O_3 the elastic modulus exhibits very little temperature dependence in the glassy state, drops precipitously above T_g but then reaches a persistent positive slope at high temperatures. Hence, at first glance B_2O_3 behaves more like a normal material, at least under ambient conditions. Conversely, the steady increase of the elastic modulus upon heating at temperatures 1000 °C above the melting point of crystalline B_2O_3 is quite unusual and indicative of a strong networking tendency in this material. Moreover, as we recently discovered, B_2O_3 also responds to applied compressive deformation with polyamorphic transitions.[18] Using concurrent Brillouin and Raman light scattering experiments, we monitored the structural developments in this material during repeated compression-decompression cycles. Structural states visited during compression and decompression are different, as revealed the hysteresis in elastic moduli. Interestingly, the transitions, which involve the changeover between three- and four-coordinated boron, are continuous during compression and discontinuous after almost completely releasing the applied pressure.

Despite its great importance as a strong network glass former, the structure of vitreous B_2O_3 is a much debated topic, particularly concerning the prevalence and structural role of boroxol (B_3O_6) groups. According to the first structural model of vitreous boron oxide proposed by Zachariasen,[20] the glass consisted of a three-dimensionally random network of BO_3 triangles. This model was chal-

lenged in 1953 when an anomalously sharp and intense line was observed in the Raman spectrum of boron oxide at 808 cm^{-1} by Gorbeau *et al.*[21] The authors suggested that the BO_3 triangles were not randomly oriented, but groups of three were bonded together into a boroxol (B_3O_6) ring. The sharp 808 cm^{-1} Raman line was assigned to the symmetric stretching mode[22] or breathing mode[23] of the boroxol ring. Ever since, the fraction f of boron atoms that can be found in boroxol rings has been a highly debatable subject. Values for f ranging from 0.5 to 0.85 have been derived from x-ray diffraction,[24] neutron diffraction,[25–27] NMR,[28,29] and Raman[30] studies. However, Dunlevey *et al.*[31] argued that the fraction of boroxol rings must be small due to a discrepancy between the radial distribution function predicted for a model glass containing a large percentage of boroxol rings and the actual radial distribution function obtained from their x-ray diffraction studies on hydrostatically compressed B_2O_3 glass. Soppe *et al.*[32] also claimed their x-ray diffraction data can be explained very well by a model containing more or less randomly connected BO_3 triangles. This claim has been supported by a number of molecular dynamics simulations[32–38] of vitreous B_2O_3 using potentials with and without three-body constraints of the B-O-B or O-B-O angles. Models with no boroxol rings were immediately criticized for their unrealistic bond angles (the B-O-B angle is about 150–160° in simulations compared to 130° in experiments) and their high densities. Later MD simulations, with the inclusion of three-body,[19,39,40] four-body,[41,42] or many-body polarization effect,[43] produce vitreous B_2O_3 structures with between 1% and 37% of the boron in boroxol rings. Similarly, recent *ab initio*[44] and reverse Monte Carlo (RMC) simulations[45,46] yield estimates for the fraction of boroxol rings between 10% and 20%. Hence, the prevailing structural model for vitreous B_2O_3 is that of a random mixture of BO_3 triangles and boroxol rings, with no clear consensus on the f value.

In this paper we will report on simulations that elucidate the structural origin of the anomalous thermomechanical behaviors of B_2O_3 glass, in particular how these anomalies are related to underlying polyamorphic transitions and what effect the concentration of boroxol rings has on this behavior. To simulate a system such as B_2O_3, in which the structural building block can exhibit multiple coordination states, it is essential to use a potential model that allows for coordination changes during simulations. Hence, we will first discuss our approach for developing such a coordination-dependent three-body potential. Then we will present the application of this potential to simulating the polyamorphic transitions in boron oxide glass. Based on this potential model, we successfully reproduce the known anomalous thermomechanical behavior of B_2O_3, i.e., the minimum in its mechanical modulus in the molten state. Furthermore, our MD simulations predict a resurfacing of this anomaly under tensile stress and ambient temperatures, and in the attempt to verify whether the underlying mechanism are universal for all network-forming glasses, we discovered previously unknown low-density crystalline polymorphs of B_2O_3.

II. COMPUTATIONAL DETAILS

A. Coordination-dependent potential model

There are three main features of our coordination-dependent charge-transfer three-body potential model: (1) *dynamic charge redistribution*—a charge transfer term controls the extent of charge polarization in a covalent bond, as well as the amount of charge transferred between atoms upon rupture or formation of such a bond; (2) *conditional three-body interactions*—the directional character of the covalent bonding in B_2O_3, modeled by means of three-body terms that constrain both B-O-B and O-B-O angles, is coupled to the degree of covalency in atomic interactions and vice versa; (3) *variable coordination number*—both two- and three-body interactions depend on the effective number of nearest neighbors of an atom, which is evaluated dynamically based on the local environment of this atom.

The interaction potential used here is based on an earlier version,[47] which for this project has been expanded to encompass multiple coordination states. It includes a Coulomb term, a Born-Huggins-Mayer repulsive term and a three-body term. The potential energy for a given particle is

$$\phi_i = q_i \sum_{j=1}^{N} \frac{q_j}{4\pi\varepsilon_0 r_{ij}} + \sum_{j=1}^{NC} C_{ij} e^{(\sigma_i+\sigma_j-r_{ij})\cdot\rho_{ij}} + \sum_{j=1}^{NC-1} \sum_{k=j+1}^{NC} (\varphi_{ij}+\varphi_{ik})\Lambda_{ijk}, \quad (1)$$

where ε_0 is the dielectric constant of vacuum, r_{ij} is the interatomic distance, q_i is the charge on atom i. σ_i is a measure of the size of the atom i, and ρ_{ij} describes the hardness in the repulsion between atoms with overlapping electron orbitals. The three-body term accounts for the directionality in covalent bonds. It comprises purely attractive terms, $\varphi_{ij}=-C_{ij}\frac{\kappa_{ij}}{\eta_{ij}}\zeta_{ij}e^{(\lambda_{ij}-r_{ij})\eta_{ij}}$, that act in radial direction between pairs of bonded atoms, and an angular constraint term, whose magnitude and equilibrium angle depend on the effective coordination number of the central atom. ζ_{ij} is a function of the interatomic spacing, which is defined below. This term couples the magnitude of the covalent attraction to the amount of charge transferred between neighboring atoms; it effectively regulates the degree of ionicity of these interactions. All other symbols represent potential parameters defined in Table I. Additional detail concerning their physical meaning may be found in Ref. 47.

To determine the effective coordination number we define two concentric spherical regions around each particle [Fig. 1(a)]. Atoms within the inside sphere are considered full neighbors of the central atom; those located in between the inner and outer sphere are considered partial neighbors, and those outside of the outer sphere are not included as neighbors. The effective coordination number Z_i of particle i is then calculated according to

$$Z_i = \sum_{j\neq i}^{NC} f(|r_{ij}|), \quad (2)$$

where NC is the total number of atoms contained within the outer cutoff sphere, and $f(|r_{ij}|)=(1+e^{(|r_{ij}|-a_Z)b_Z})^{-1}$ is a func-

TABLE I. Optimized potential parameters for boron oxide.

Element		σ_i (nm)			n_i	z_i				$q_i^{\emptyset}$
B		0.0740			2	+3				+2.4
O		0.1470			8	−2				−1.6
Pair	A_{ij} (10^{-19} J)	ρ_{ij} (nm^{-1})			λ_{ij} (nm)	η_{ij} (nm^{-1})				κ_{ij} (nm^{-1})
B-B	0.3042	33.0			0.000	0.0				33.0
B-O	0.1578	34.4			2.602	2.5				30.4
O-O	0.3312	39.0			0.000	0.0				38.0
Charge transfer		Δ_{ij} (e)	a_C (nm)	b_C (nm^{-1})						
		0.1270	0.38	10						
Triplet		γ_{ijk} (rad^{-2})	$\bar{\theta}$ (deg)							
B-O-B		0.100	120							
Coordination	a_Z (nm)	b_Z (nm^{-1})	C_3	C_4	A_3	A_4	γ_3 (rad^{-2})	γ_4 (rad^{-2})	$\bar{\theta}_3$ (deg)	$\bar{\theta}_4$ (deg)
O-B-O	0.22	100	1.0	0.3	2.00	2.00	0.05	0.05	120	109.5

tion that varies continuously between 1 at short distance and 0 at large distance and describes the contribution that each particle makes towards the effective coordination number [Fig. 1(a)]. The parameters a_Z and b_Z are adjusted so that this function reaches the two limiting values at the radius of the inner and outer coordination region respectively. Accordingly, the effective coordination number may be noninteger. When an atom m is approaching the central atom i, which is already surround by three other atoms j, k, and l, either a bond exchange or a coordination change may take place. During such changeovers, the energy of the configuration must vary continuously, and we accomplish this by constructing the energy term for the angular part of the potential to not only depend on the angle formed by a given the triplet $\langle ijk \rangle$, but also on the effective coordination number Z_i of the central atom, i.e.

$$\Lambda_{ijk} = \sum_{Z_0=3}^{6} C_{Z_0} e^{-A_{Z_0}(Z_0 - Z_i)^2} e^{-\gamma_{Z_0}(\bar{\theta}_{Z_0} - \theta_{ijk})^2}, \tag{3}$$

where θ_{Z_0} is the equilibrium angle of the triplet in one of the fundamental coordination environments. For example, three- and four-coordinated species will tend to form sp^2 and sp^3 hybridized bonds with equilibrium angle $\bar{\theta}_3 = 120°$ and $\bar{\theta}_4 = 109.5°$, respectively. C_{Z_0}, A_{Z_0}, and γ_{Z_0} control the depth of the potential well, the coordination-dependent width, and the angle-dependent width of the three-body potential, respectively. These three parameters can be adjusted so that the depths and widths of the potential well are the same for all possible coordination states, or certain coordination states could be favored over others. A typical multiwell potential function is illustrated in Fig. 1(b). Λ_{ijk} and its first and second derivatives are continuous, which allow atoms to smoothly transition from one coordination environment to another. Furthermore, unlike the environment-dependent interatomic potentials developed for silicon and carbon,[48–50] our potential will not break down for noninteger coordination numbers. In our model, nearest neighbor configurations in between well-defined coordination states, e.g., trigonal, tetrahedral, etc., are characterized by the higher energies of transition states and have much reduced angular constraints, which allows for a swift changeover between different coordination geometries.

As a result of breaking or forming covalent bonds, charge transfer takes place between the central atom and all NC atoms within the outer radius of the coordination environment. The net charge associated with atom i is calculated according to

$$q_i = q_i^{\emptyset} - 2\sum_{j=1}^{NC} \Delta_{ij}\zeta_{ij}, \tag{4}$$

where $q_i^{\emptyset}$ is the charge of the isolated atom and $\zeta_{ij} = (1 + e^{b_c(r_{ij} - a_c)})^{-1}$ is the charge transfer function. a_c and b_c are empirical parameters. Electroneutrality is assured by requiring that $\Delta_{ij} = -\Delta_{ji}$. The net charge on the atoms will decrease with the increase of coordination number (the charges on B ions change from +1.7 to +1.48 in their threefold and fourfold coordinated states, respectively), which in turn will reduce the strength of the atomic interactions in the direction of the bond, or vice versa. This dependence is consistent with theoretical calculations which have demonstrated that bond strengths decrease and bond lengths increase with increasing coordination number.[51] Due to its simplicity and the fact that it preserves generality and the basic physics, our potential can be easily adopted to study a variety of reactive systems, especially when they include species that undergo different hybridizations.

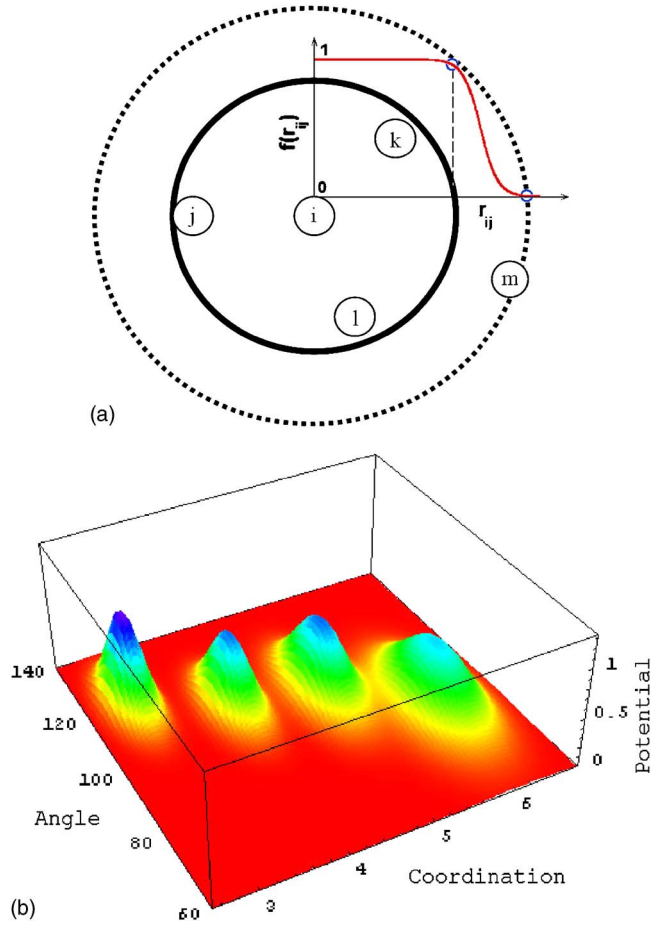

FIG. 1. (Color online) (a) Sketch of the neighbor-cutoff spheres and the function to determine the effective coordination number Z_i of the central particle i. (b) Graphical representation of the three-body potential term as a function of the angle between adjacent bonds and the effective coordination number. Negative energies are plotted upwards for better visualization.

B. Parametrization of the potential parameters

An initial parametrization of this force field was done by matching the density, bond length, and bond angle of crystalline α-B_2O_3 to experimental values. The parameters were further adjusted to achieve the best possible agreement of density, radial distribution function, structure factor, bond angle distribution, vibrational density of states, and infrared spectra of molten B_2O_3 with experimental data. The parameters for the coordination-dependent part were adjusted so that the coordination of boron in crystalline α-B_2O_3 is 3 at ambient conditions and starts to change from 3 to 4 at approximately 3 GPa, i.e., the pressure at which α-B_2O_3 transforms in β-B_2O_3 in experiments. In the present study, the coordination-dependent three-body potential is only used for O-B-O triplets, not for B-O-B triplets, and Z_0 is summed from 3 to 4 in Eq. (3). The values of various parameters for boron oxide are summarized in Table I. The cutoff for the Coulombic interaction is 10.6 Å, and for the short range interaction between B-B, B-O, and O-O is 3, 2, and 3 Å, respectively.

C. Preparation of initial glass and details of MD simulations

To generate initial B_2O_3 glass, we started from cesium enneaborate ($Cs_2O.9B_2O_3$) crystal,[52] which has both boroxol groups and triborate groups. After extracting Cs_2O and some BO_3 triplets, a unit cell of 80 atoms is obtained, which has 75% B atoms inside boroxol rings.[53,54] MD simulations were carried out for 640-atom (256 B and 384 O) and 2560-atom (1024 B and 1536 O) systems with periodic boundary conditions. No system size effects in excess of statistical errors could be detected between the two. These systems were equilibrated at 2500 K, under which condition the boroxol rings gradually dissolve. Hence, by heat treating the system for various periods of time, up to a nanosecond, B_2O_3 liquids with 75%, 63%, 50%, and 10% of the B atoms inside the boroxol rings, were generated. These liquids were subsequently quenched at a rate of 2.5 K/ps to get initial glass samples. Experiments show that the fraction of boroxol rings increases with decreasing temperature.[55] However, in MD simulations, no additional boroxol rings are generated upon cooling because the extremely high quench rates do not allow for the necessary reactions and structural relaxation to take place. For systems with between 10% and 75% boroxol rings, the density at ambient conditions ranges from 1.75 to 1.81 g/cm^3, which is very close to the experimental value of 1.80 g/cm^3 for B_2O_3 glass.[25] The total and partial structure factor $S(Q)$ of the sample with 63% boroxol rings are plotted in Fig. 2(a). Superimposed onto the total $S(Q)$ is that for the sample with 10% boroxol rings. The total structure factors of the two systems are very close to each other, except that the small peak between the first and second main peak, which in the sample with 10% boroxol ring is slightly lower than that of the sample with 63%. These total and partial $S(Q)$ are in good agreement with experimental data [Fig. 2(b)].[24,46,56] No remnants of the initial crystalline structure was found in the glasses prepared this way. However, since B_2O_3 liquids with different amounts of boroxol rings were equilibrated at 2500 K for different durations, those with high boroxol ring concentration may not have been fully relaxed before they were quenched. So no attempt is made to establish the relation between density and boroxol ring concentration of initial B_2O_3 glasses. Nevertheless, our study shows that B_2O_3 glasses with a large range of boroxol ring concentrations can be made in MD simulations, which have both density and structure factors close to experimental data.

The hydrostatic compression-decompression was carried out at 300 K, between −20 GPa and 50 GPa, at 1 GPa intervals. The rate of compression was 0.5 GPa/ps. Temperature ramping was achieved by velocity scaling and the density adjusts according to the Anderson constant-pressure algorithm.[57] The bulk modulus of B_2O_3 glass was calculated directly from the equation of state according to $B=\rho(dP/d\rho)$.

III. RESULTS AND DISCUSSION

Figure 3(a) shows the evolution of density and bulk modulus of our simulated B_2O_3 glass with temperature. For

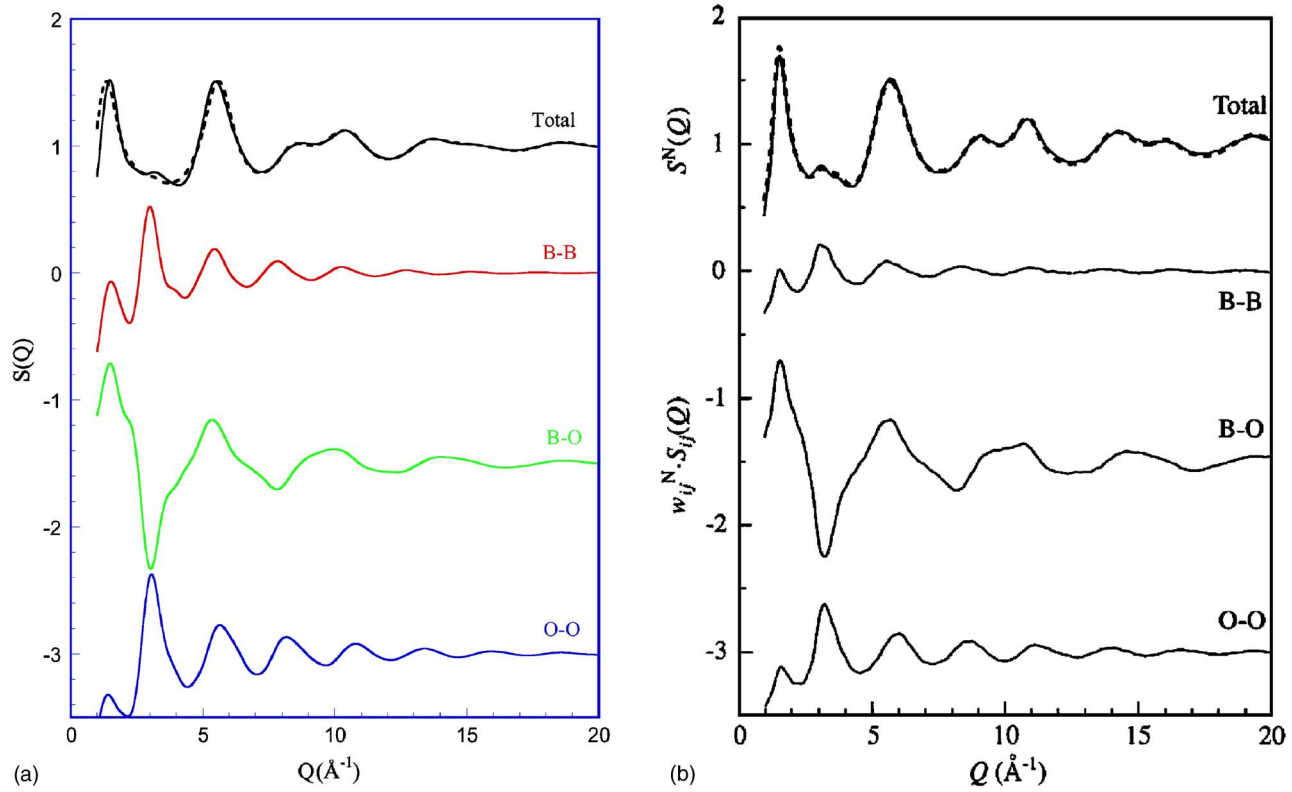

FIG. 2. (Color online) Total and partial structure factor $S(Q)$ for vitreous B_2O_3 generated using MD simulations (a), those from reverse Monte Carlo (RMC) results (full lines) in comparison with the total structure factor from neutron scattering experiments (dashed line) (b) (Ref. 46). In panel (a), the total $S(Q)$ for a simulated glass containing 10% of boron atoms in boroxol rings (dashed line) is superimposed onto that of a glass containing 63% of boron atoms in boroxol rings (full line).

comparison, the elastic modulus vs temperature data of network-forming glasses, as measured by Brillouin scattering experiments,[19] is shown in Fig. 3(b). In this plot, the aforementioned anomalous increases in the elastic moduli, and the universality of this behavior for all three major network glass formers are apparent. Note that GeO_2 essentially echoes the behavior of SiO_2, albeit with a hint of structural reorganization just above T_g. In contrast, B_2O_3 exhibits a behavior that differs in two substantial ways: the positive temperature dependence of the modulus is not present in the room-temperature glass, and the drop in elastic modulus above T_g is significantly more pronounced than even for GeO_2. In previous studies,[3–6] we successfully reproduced these anomalous behaviors for silica glass and revealed the underlying structural origin. Since SiO_2 and GeO_2 are structurally very similar, e.g., the cation is four coordinated by O atoms at ambient conditions, we expect that the mechanisms responsible for the anomalies of GeO_2 to differ from those in SiO_2 only by nuances. The case of B_2O_3, as a representative of three-coordinated systems, is therefore far more intriguing. Figure 3(a) shows that, irrespective of the concentration of boroxol rings in the initial vitreous B_2O_3, right above the glass transition temperatures indicated by vertical arrows, the bulk modulus decreases first, and then increases again with the increase of temperature. This is in excellent agreement with experimental data in Fig. 3(b). Hence, in B_2O_3 the anomalous behavior is shifted to higher temperatures.

To identify what causes the anomalies in B_2O_3, and in fact establish that the underlying mechanisms are in essence ubiquitous to all strongly networked glasses, we used simulations to explore the behavior of this material under conditions that are difficult, if not impossible to realize in experiments. In our previous studies we demonstrated that the effects of thermal and mechanical influences are equivalent, i.e., silica glass becomes stiffer when its structure expands, regardless of whether the expansion is achieved via heating or by applying a tensile stress. Next we will therefore examine how the mechanical moduli of vitreous B_2O_3 change in response to stress. Note that the anomalous behavior for B_2O_3 only sets in at high temperatures, i.e., when the structure is expanded to a significant degree. Hence, in order to incite this behavior mechanically, we must explore the tensile stress regime as well.

The influence of the initial boroxol ring concentration on the pressure dependence of the elastic modulus is barely discernable. In the positive pressure range in Fig. 4, upon compression, both density and bulk modulus smoothly increase with pressure, and upon decompression they follow a different path, exhibiting higher magnitudes and less pressure dependence. During decompression, the bulk modulus decreases smoothly until ~2–3 GPa, upon which the bulk modulus returns to values followed during compression to form a closed hysteresis loop. However, the density of the recovered glasses does not return to its initial value, indicating a permanent densification throughout the compression-decompression cycle due to irreversible amorphous-amorphous transitions. Structural analysis shows that boron gradually converts from three- to four-coordinated units

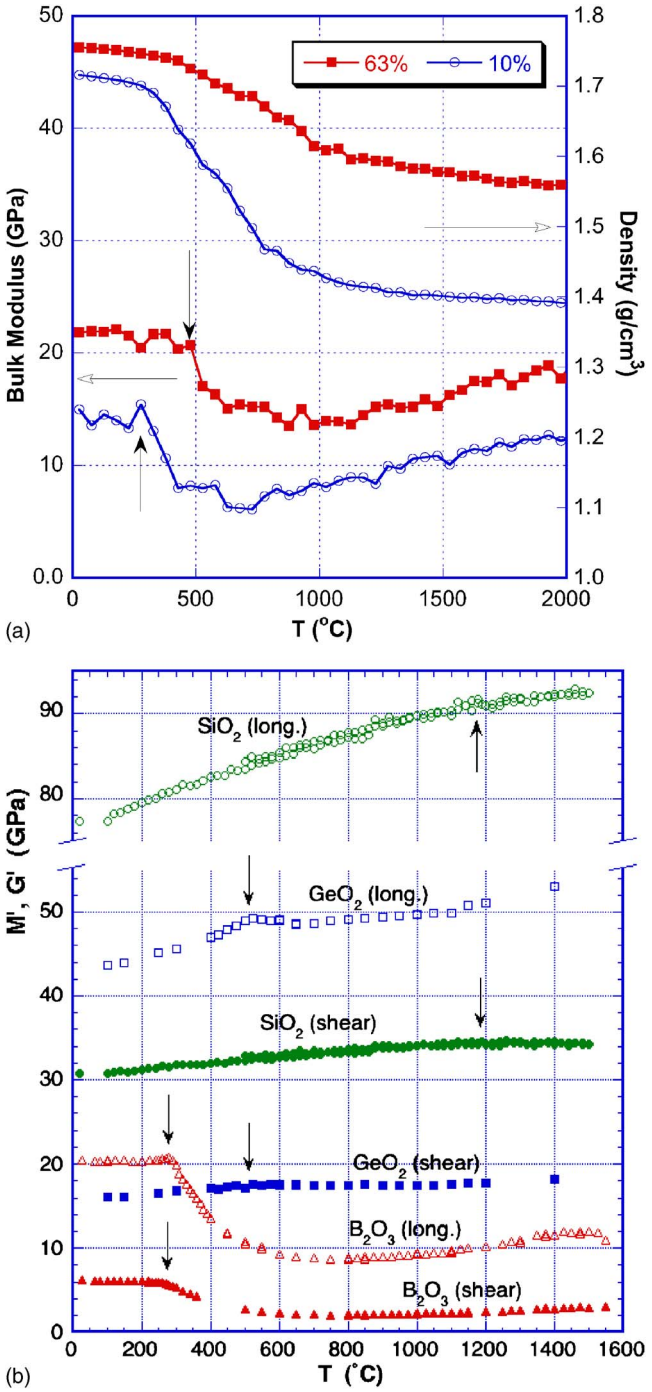

FIG. 3. (Color online) The evolution of elastic moduli of B_2O_3 glass with temperature from MD simulations (a) compared to that in Brillouin scatting experiments (b) (Ref. 19).

upon compression, a transformation that completely reverts upon decompression, albeit with some hysteresis. This is in agreement with the experimental observations by Wright *et al.*,[56] who found that there is no coordination change in permanently densified vitreous B_2O_3. Hence, our MD simulations confirm that the polyamorphic transitions in three-coordinated B_2O_3 glass involve transitory four-coordinated boron atoms at high pressures, while coordination change is not necessary for permanent compaction of the recovered

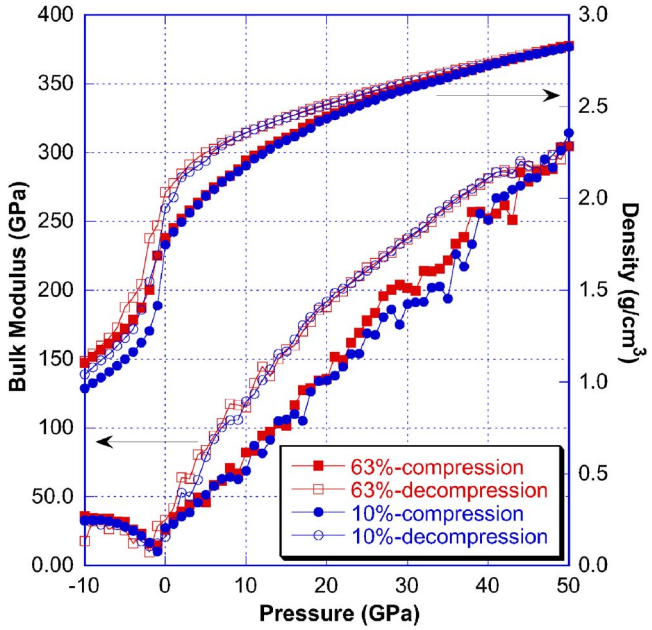

FIG. 4. (Color online) Change in density and bulk modulus of simulated B_2O_3 glasses with pressure during compression and decompression.

glass. In contrast, our previous MD simulations show that a coordination change is not required for the densification of silica glass compressed up to 20 GPa. In general the trends we observe in simulations all echo those observed in experiments.[16–18,58] A detailed comparison of the behavior of simulated B_2O_3 glass under high pressure with the results of our light scattering experiments will be published elsewhere. Here we concentrate on the tensile regime.

Figure 4 shows that the bulk modulus of both original and recovered glass at first continues to decrease when expanded under isotropic tensile stress. After reaching a minimum at about −1 GPa, the modulus increases again, i.e., the pressure dependence of the elastic modulus becomes negative. It is the first time, to our knowledge, that this anomaly is observed in three-coordinated B_2O_3 glass. Hence, there appear to be some definite parallels in the modulus vs pressure behaviors of three- and four-coordinated network glasses. While the bulk modulus minimum in silica glass is at ~2–3 GPa, which can be easily measured by experiments,[59–62] in B_2O_3 glass the minimum occurs at a negative pressure, and has so far eluded experiments. Our simulations also show that the minimum for B_2O_3 shifts toward the positive pressure range at higher temperatures, which is consistent with the notion that the occurrence and extent to which the network structures behave anomalously can be sensibly mapped onto a density change, whether this is brought on by thermal expansion or tensile stress. For each glass-forming system, the anomalous negative modulus vs density dependence intercepts normal behavior and consequently extends between a maximum and a minimum. Silica glass behaves anomalously at ambient conditions. At room temperature, the maximum therefore occurs at negative and the minimum at positive pressures, and because of the small expansion coefficient of this substance, the anomalous be-

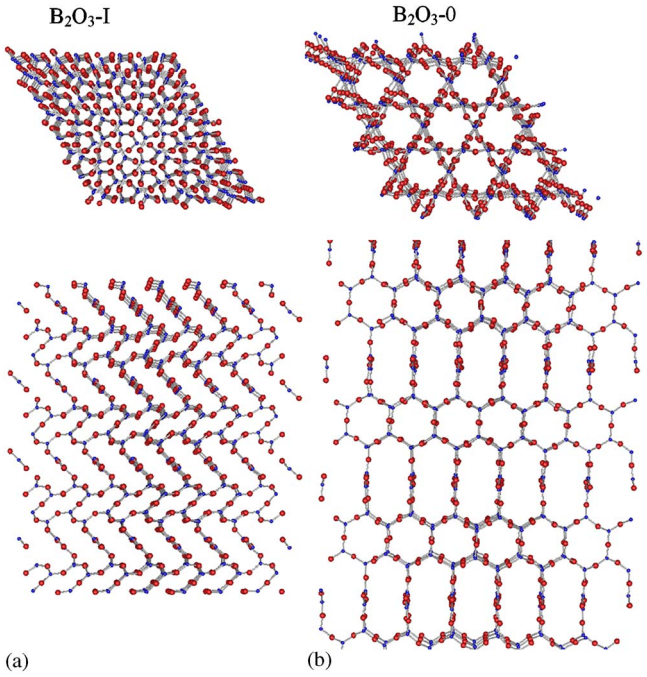

FIG. 5. (Color online) Structure of B_2O_3-I (a) and low-density B_2O_3-0 crystal (b). Note: the large spheres are O atoms; the small ones are B atoms. Views are along [001] (top) and [110] (bottom) directions of B_2O_3-I crystal, respectively.

havior persists over a wide temperature range at ambient pressure. In vitreous B_2O_3 the anomalous regime is shifted towards negative pressures at room temperature, but due to a larger thermal expansion coefficient, the anomalous behavior resurfaces at high temperature under ambient pressure. Our results show that the anomalous increase of the elastic moduli upon expansion are one and the same whether brought upon by tensile deformation or thermal expansion, and that it is a universal trait of network-forming glasses, tetrahedral and trigonal. Moreover, the phenomenon appears to be unaffected by the glass transition, i.e., it persists from the glassy into the liquid state. We will now complete our analysis by uncovering a possible explanation for the structural origin of this anomaly in B_2O_3 glass that is consistent with what we have found for tetrahedral networks.

With our previous MD simulations we demonstrated that the thermomechanical anomalies in silica glass are due to reversible polyamorphic transitions, essentially echoing the structural transformations in its crystalline counterparts by invoking modes of displacement of the structural units that are similar to those underlying the α-to-β transformation in cristobalite silica, and by creating ring configurations in the dense and expanded glass that have similar characteristics as those in α- and β-cristobalite, respectively. The higher elastic modulus of β-cristobalite is due to a more symmetric orientation of bonds as compared to α-cristobalite. In the former, deformation entails bond compression and bending modes that offer equal resistance in all directions, whereas in the latter, due to bond pivoting, rings can twist and compliantly fold up onto themselves when compressed. Silica glass is made of a mixture of local structural motifs with α- and β-like rings, i.e., close to those in high-density low-modulus α-cristobalite and low-density high-modulus β-cristobalite, respectively. Accordingly, compressive volume changes of silica glass lead to the collapse of the network rings, which assume α-like geometries, and hence the structure softens. Conversely, upon expansion the local network character changes from α-like to β-like, and the bulk modulus increases. To argue that anomalous thermomechanical properties are universal for all network glasses, a similar transition-based mechanism must be responsible for the behavior of vitreous B_2O_3. The question then arises as to what might be the local structural motifs, and whether corresponding crystalline counterparts exist.

Two crystalline forms are known for boron oxide, i.e., B_2O_3-I, which is stable at ambient pressures and has boron coordinated by three oxygen atoms, and B_2O_3-II, which is stable at higher pressure and has tetrahedrally coordinated boron. B_2O_3-I falls within the trigonal space group of $P3_1$,[63] and has a density of 2.56 g/cm^3, much higher than 1.80 g/cm^3 of B_2O_3 glass.[25] Views of the B_2O_3-I structure along the [001] and [110] crystallographic directions are shown in Fig. 5(a). Subject to tensile isotropic stress our simulated B_2O_3-I expands and at −6 GPa transforms into a low-density phase with a monoclinic space group of $C121$. We tentatively call this phase B_2O_3-0 in light of the succession it assumes in terms of density relative to B_2O_3-I and B_2O_3-II. B_2O_3-0 has a very open structure, as seen either

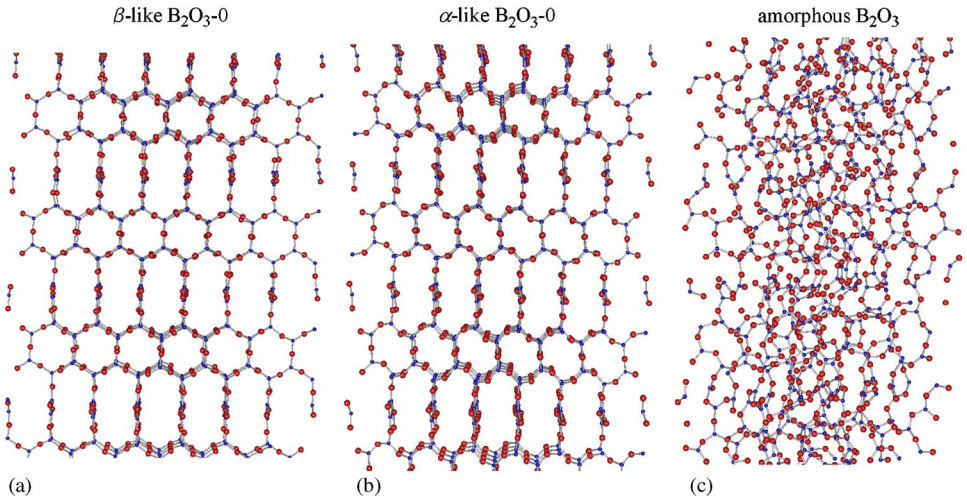

FIG. 6. (Color online) Structure of β-like B_2O_3-0 (a) and α-like B_2O_3-0 crystal (b). Amorphous B_2O_3 (c) can be made of local structure motifs similar to β-like and α-like B_2O_3-0 crystal. Note: the large spheres are O atoms; the small ones are B atoms. All the structures are viewed along the [010] direction of B_2O_3-0 crystal.

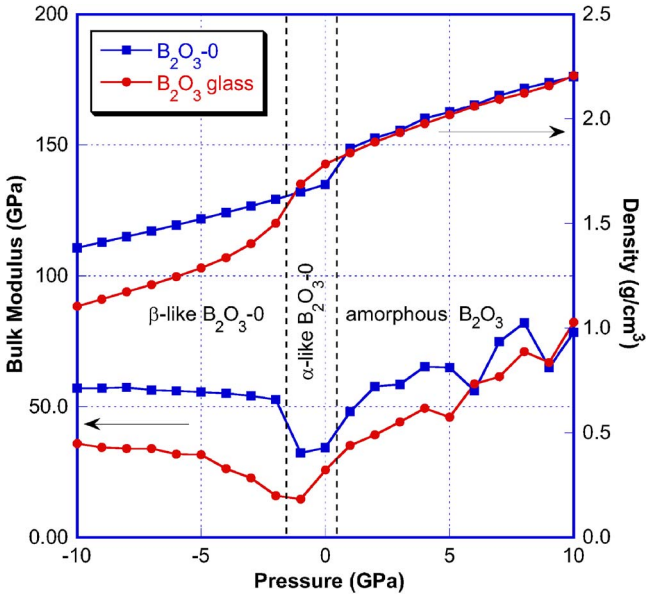

FIG. 7. (Color online) Change in density and bulk modulus of B_2O_3 glass and B_2O_3-0 crystals under pressure. Stability ranges of α-like B_2O_3-0 and β-like B_2O_3-0 are delineated.

from the top or side view in Fig. 5(b). Furthermore, upon releasing the tensile stress, B_2O_3-0 does not revert to B_2O_3-I but instead undergoes another structural transition at −2 GPa that results in the partial collapse of network rings but almost no detectable densification beyond what can be associated with elastic deformation. Figure 6(a) and 6(b) show views of the low- and high-density modifications of B_2O_3-0 along the [010] direction. The partial collapse of network rings is particularly obvious for the smaller ring seen from this perspective. In fact, the resemblance to the ring geometries in α- and β-cristobalite is remarkable,[64] and we therefore refer to the low- and high-density modifications of B_2O_3-0 as β-like to α-like, respectively. Further compression results in the amorphization of B_2O_3-0 at about 1 GPa [Fig. 6(c)]. Figure 7 shows that the density of B_2O_3-0 is much closer to that of B_2O_3 glass at ambient pressure than that of B_2O_3-I. Similar

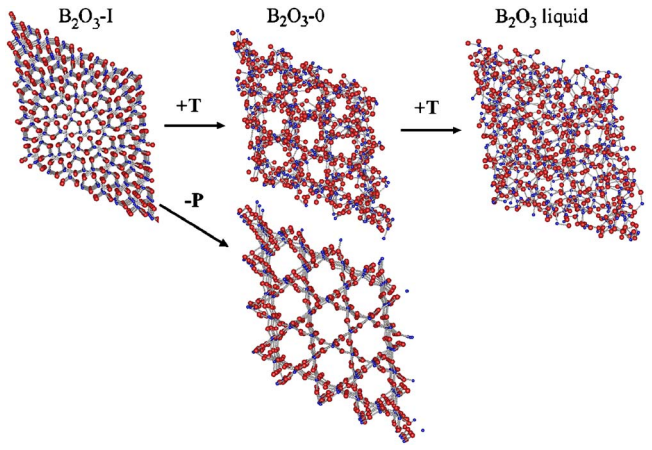

FIG. 8. (Color online) Structural transitions in crystalline B_2O_3 upon heating and mechanical expansion. Note: the large spheres are O atoms; the small ones are B atoms.

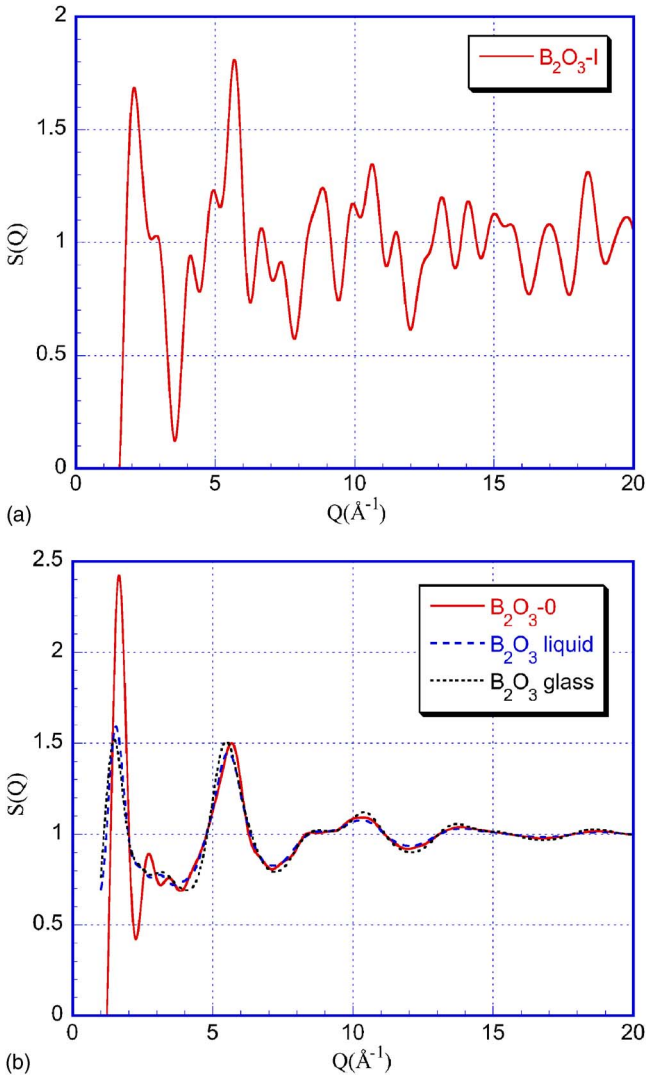

FIG. 9. (Color online) Total structure factor of B_2O_3-I crystal (a) and of B_2O_3-0 crystal at high temperature compared to that of B_2O_3 liquid, resulting from melting B_2O_3-0, and glass containing 63% of boron atoms in boroxol rings (b).

to β-cristobalite, β-like B_2O_3-0 not only has more symmetric rings, but also the higher bulk modulus of the two modifications (Fig. 7). Amorphous B_2O_3 can be thought of as a mixture of "puffed" β-like and "puckered" α-like rings. Accordingly, compression converts "puffed" rings into "puckered" rings, causing the structure to compact and soften. Conversely, upon expansion the network rings puff up and the structure stiffens. The bulk modulus of B_2O_3 glass increases gradually as it expands under tension due to the increasing population of β-like rings in the system.

Not only can the low-density B_2O_3-0 crystalline phase be introduced mechanically, but also thermally. Figure 8 shows that upon heating, B_2O_3-I transforms into B_2O_3-0 before it finally melts. The thermally introduced B_2O_3-0 at ambient pressure has an open structure similar to that of the pressure-introduced one at ambient temperature, but is much more disordered. The total structure factor of B_2O_3-I is plotted in Fig. 9(a), consisting of many peaks, typical of a crystalline structure. After the transformation, the total structure factor

of B_2O_3-0 at high temperature is very close to that of B_2O_3 liquid and of B_2O_3 glass with 63% boroxol rings [Fig. 9(b)]. The discovery of the low-density B_2O_3-0 polymorphs provides a key to uncovering the mystery of the "B_2O_3 crystallization anomaly:" B_2O_3 has never been observed to crystallize from a dry melt at ambient pressure. Even if the melt is seeded with crystals, and the crystals are melted back a bit, no crystal growth is observed at any imposed undercooling without pressure.[65,66] Since the local structure of B_2O_3 liquid is closer to that of B_2O_3-0 crystals than that of B_2O_3-I, the former will probably nucleate first from the melts upon cooling. Further cooling, however, renders B_2O_3-0 unstable at ambient pressure. At the same time, the thermal energy needed for the structural rearrangements to convert to B_2O_3-I is withdrawn and B_2O_3 is arrested in an amorphous state, perhaps containing residual fragments of B_2O_3-0. Only by applying pressure can the nucleation of B_2O_3-0 be avoided, which explains why a pressure is always needed for B_2O_3-I crystal to form from B_2O_3 liquid. If substantiated, the prediction of the crystalline B_2O_3-0 phase may have important ramifications for understanding the structure and properties vitreous B_2O_3, particularly with respect to the existence of the boroxol rings.

IV. CONCLUSIONS

Based on a newly-developed coordination-dependent charge-transfer potential, we studied the polyamorphic transitions in B_2O_3 glass under various thermomechanical conditions by using MD simulations. Our simulations demonstrate that anomalous thermomechanical behaviors, such as an increase of the mechanical moduli upon expansion, whether this is the result of tensile deformation or thermal expansion, are universal in network-forming glasses. These anomalous behaviors of network-forming glasses are due to the polyamorphic transitions between different amorphous states with local structures of different stiffness that are similar to those in the materials' crystalline counterparts. Our simulations also predict the existence of previously unknown low-density B_2O_3 polymorphs. These not only provide contrasting structural motifs for vitreous B_2O_3 that can explain its thermomechanical anomalies, but also shed new light on the mystery of the B_2O_3 crystallization anomaly.

ACKNOWLEDGMENTS

The authors acknowledge the support of National Institute of Standards and Technology, under Grant No. 60NANB9D0102 and of the National Science Foundation under Grant No. DMR-0230662. Most of the work was done on supercomputers of the Center for Advanced Computing (CAC) at the University of Michigan. L.H. would like to thank Yunfeng Shi at the University of Michigan for helpful discussions on the force field, and Linn Hobbs at MIT for stimulating discussions on the initial results.

*Electronic mail: kieffer@umich.edu

[1] G. K. White, Phys. Rev. Lett. **34**, 204 (1975).
[2] J. E. Shelby, *Introduction to Glass Science and Technology* (The Royal Society of Chemistry, Cambridge, UK, 1997).
[3] L. Huang and J. Kieffer, Phys. Rev. B **69**, 224203 (2004).
[4] L. P. Huang and J. Kieffer, Glass Sci. Technol. (Offenbach, Ger.) **77**, 124 (2004).
[5] L. Huang and J. Kieffer, Phys. Rev. B **69**, 224204 (2004).
[6] L. P. Huang, L. Duffrene, and J. Kieffer, J. Non-Cryst. Solids **349**, 1 (2004).
[7] O. Mishima, L. D. Calvert, and E. Whalley, Nature (London) **310**, 393 (1984).
[8] O. Mishima, L. D. Calvert, and E. Whalley, Nature (London) **314**, 76 (1985).
[9] O. Mishima, K. Takemura, and K. Aoki, Science **254**, 406 (1991).
[10] O. Mishima, J. Chem. Phys. **100**, 5910 (1994).
[11] M. Grimsditch, Phys. Rev. Lett. **52**, 2379 (1984).
[12] M. Grimsditch, Phys. Rev. B **34**, 4372 (1986).
[13] M. Grimsditch, R. Bhadra, and Y. Meng, Phys. Rev. B **38**, 7836 (1988).
[14] M. Grimsditch, A. Polian, and A. C. Wright, Phys. Rev. B **54**, 152 (1996).
[15] E. G. Ponyatowsky and O. I. Barkalov, Mater. Sci. Rep. **8**, 147 (1992).
[16] J. D. Nicholas, R. E. Youngman, S. V. Sinogeikin, J. D. Bass, and J. Kieffer, Phys. Chem. Glasses **44**, 249 (2003).
[17] J. D. Nicholas, S. V. Sinogeikin, J. Kieffer, and J. D. Bass, J. Non-Cryst. Solids **349**, 30 (2004).
[18] J. Nicholas, S. Sinogeikin, J. Kieffer, and J. Bass, Phys. Rev. Lett. **92**, 215701 (2004).
[19] R. E. Youngman, J. Kieffer, J. D. Bass, and L. Duffrène, J. Non-Cryst. Solids **222**, 190 (1997).
[20] W. H. Zachariasen, J. Am. Chem. Soc. **54**, 3841 (1932).
[21] J. Goubeau and H. Keller, Z. Anorg. Allg. Chem. **272**, 303 (1953).
[22] F. L. Galeener, Solid State Commun. **44**, 1037 (1982).
[23] J. Krogh-Moe, J. Non-Cryst. Solids **1**, 269 (1969).
[24] R. L. Mozzi and B. E. Warren, J. Appl. Crystallogr. **3**, 251 (1970).
[25] P. A. V. Johnson, A. C. Wright, and R. N. Singlair, J. Non-Cryst. Solids **50**, 281 (1982).
[26] A. C. Hannon, D. I. Grimley, R. A. Hulme, A. C. Wright, and R. N. Sinclair, J. Non-Cryst. Solids **177**, 299 (1994).
[27] R. N. Sinclair, C. E. Stone, A. C. Wright, I. G. Polyakova, N. M. Vedishcheva, B. A. Shakhmatkin, S. A. Feller, B. C. Johanson, P. Venhuizen, R. B. William, and A. C. Hannon, Phys. Chem. Glasses **41**, 286 (2000).
[28] G. E. Jellison, L. W. Panek, P. J. Bray, and G. B. Rouse, J. Chem. Phys. **66**, 802 (1977).
[29] C. Joo, U. Werner-Zwanziger, and J. W. Zwanziger, J. Non-Cryst. Solids **261**, 282 (2000).
[30] G. E. Walrafen, Y. C. Chu, and M. S. Hokmabadi, J. Chem. Phys. **92**, 6987 (1990).

[31] F. M. Dunlevey and A. R. Cooper, in *Structure of Noncrystalline Materials*, edited by P. H. Gaskell (Taylor & Francis Ltd, London, 1977), p. 211.
[32] W. Soppe, C. van der Marela, W. F. van Gunsteren, and H. W. den Hartog, J. Non-Cryst. Solids **103**, 201 (1988).
[33] W. Soppe and H. W. den Hartog, J. Phys. C **21**, L689 (1988).
[34] W. Soppe and H. W. den Hartog, J. Non-Cryst. Solids **108**, 260 (1989).
[35] Q. Xu, K. Kawamura, and T. Yokokawa, J. Non-Cryst. Solids **104**, 261 (1988).
[36] A. H. Verhoef and H. W. den Hartog, Radiat. Eff. Defects Solids **119-121**, 493 (1991).
[37] A. H. Verhoef and H. W. den Hartog, J. Non-Cryst. Solids **146**, 267 (1992).
[38] A. H. Verhoef and H. W. den Hartog, J. Non-Cryst. Solids **180**, 102 (1994).
[39] H. Inoue, N. Aoki, and I. Yasui, J. Am. Ceram. Soc. **70**, 622 (1987).
[40] A. Takada, C. R. A. Catlow, and G. D. Price, J. Phys.: Condens. Matter **7**, 8693 (1995).
[41] R. Fernández-Perea, F. J. Bermejo, and M. L. Senent, Phys. Rev. B **54**, 6039 (1996).
[42] R. Fernández-Perea, F. J. Bermejo, and E. Enciso, Phys. Rev. B **53**, 6215 (1996).
[43] J. K. Maranas, Y. Z. Chen, D. K. Stillinger, and F. H. Stillinger, J. Chem. Phys. **115**, 6578 (2001).
[44] M. Teter, in *Proceedings of the Second International Conference on Borate Glasses, Crystals, and Melts*, 1996, p. 407.
[45] J. Swenson and L. Börjesson, Phys. Rev. B **55**, 11138 (1997).
[46] K. Suzuya, Y. Yoneda, S. Kohara, and N. Umesaki, Phys. Chem. Glasses **41**, 282 (2000).
[47] L. P. Huang and J. Kieffer, J. Chem. Phys. **118**, 1487 (2003).
[48] M. Z. Bazant, E. Kaxiras, and J. F. Justo, Phys. Rev. B **56**, 8542 (1997).
[49] A. Saguia, B. Boechat, and M. A. Continentino, Phys. Rev. B **58**, 58 (1998).
[50] N. A. Marks, Phys. Rev. B **63**, 035401 (2001).
[51] J. R. Chelikowsky, J. C. Phillips, M. Kamal, and M. Strauss, Phys. Rev. Lett. **62**, 292 (1989).
[52] J. Krogh-Moe and M. Ihara, Acta Crystallogr. **23**, 427 (1967).
[53] A. Takada, C. R. A. Catlow, and G. D. Price, Phys. Chem. Glasses **44**, 147 (2003).
[54] A. Takada, Phys. Chem. Glasses **45**, 156 (2004).
[55] A. K. Hassan, L. M. Torell, L. Börjesson, and H. Doweidar, Phys. Rev. B **45**, 12797 (1992).
[56] A. C. Wright, C. E. Stone, R. N. Sinclair, N. Umesaki, N. Kitamura, K. Ura, N. Ohtori, and A. C. Hannon, Phys. Chem. Glasses **41**, 296 (2000).
[57] H. C. Andersen, J. Chem. Phys. **72**, 2384 (1980).
[58] S. K. Lee, P. J. Eng, H. K. Mao, Y. Meng, M. Newville, M. Y. Hu, and J. F. Shu, Nat. Mater. **4**, 851 (2005).
[59] P. W. Bridgman, Am. J. Sci. **10**, 359 (1925).
[60] P. W. Bridgman, Proc. Am. Acad. Arts Sci. **76**, 9 (1945).
[61] P. W. Bridgman, Proc. Am. Acad. Arts Sci. **76**, 71 (1948).
[62] O. B. Tsiok, V. V. Brazhkin, A. G. Lyapin, and L. G. Khvostantsev, Phys. Rev. Lett. **80**, 999 (1998).
[63] G. E. Gurr, P. W. Montgomery, C. D. Knutson, and B. T. Gorres, Acta Crystallogr. **B26**, 906 (1970).
[64] L. Huang and J. Kieffer, Phys. Rev. Lett. **95**, 215901 (2005).
[65] M. J. Aziz, E. Nygren, J. F. Hays, and D. Turnbull, J. Appl. Phys. **57**, 2233 (1985).
[66] D. R. Uhlmann, J. F. Hays, and D. Turnbull, Phys. Chem. Glasses **8**, 1 (1967).